AGU PUBLICATIONS

Geophysical Research Letters

RESEARCH LETTER
10.1002/2015GL063349

Key Points:
- We report the characteristics of PMWE from the PANSY radar observations in 2013
- Monthly mean PMWE in a height-time section was shown from March to September
- PMWE was detected in the altitude range of 72–78 km for 2–3 h after sunset

Correspondence to:
T. Nishiyama,
nishiyama.takanori@nipr.ac.jp

Citation:
Nishiyama, T., K. Sato, T. Nakamura, M. Tsutsumi, T. Sato, M. Kohma, K. Nishimura, Y. Tomikawa, M. K. Ejiri, and T. T. Tsuda (2015), Height and time characteristics of seasonal and diurnal variations in PMWE based on 1 year observations by the PANSY radar (69.0°S, 39.6°E), *Geophys. Res. Lett.*, *42*, 2100–2108, doi:10.1002/2015GL063349.

Received 13 FEB 2015
Accepted 5 MAR 2015
Accepted article online 10 MAR 2015
Published online 3 APR 2015

Height and time characteristics of seasonal and diurnal variations in PMWE based on 1 year observations by the PANSY radar (69.0°S, 39.6°E)

Takanori Nishiyama[1], Kaoru Sato[2], Takuji Nakamura[1,3], Masaki Tsutsumi[1,3], Toru Sato[4], Masashi Kohma[2], Koji Nishimura[1], Yoshihiro Tomikawa[1,3], Mitsumu K. Ejiri[1,3], and Takuo T. Tsuda[5]

[1]National Institute of Polar Research, Tachikawa, Japan, [2]Department of Earth and Planetary Science, University of Tokyo, Tokyo, Japan, [3]Department of Polar Science, SOKENDAI (Graduate University for Advanced Studies), Tachikawa, Tokyo, Japan, [4]Department of Communications and Computer Engineering, Kyoto University, Kyoto, Japan, [5]Department of Communication Engineering and Informatics, University of Electro-Communications, Tokyo, Japan

Abstract We report height and time variations in polar mesosphere winter echoes (PMWE) based on the Program of the Antarctic Syowa mesosphere-stratosphere-troposphere/incoherent scatter (PANSY) radar observations. PMWE were identified for 110 days from March to September 2013. PMWE occurrence frequency increased abruptly in May when two solar proton events occurred. PMWE were also observed even during periods without any solar proton events, suggesting that a possible cause of the PMWE is ionization by energetic electron precipitations. The monthly mean PMWE characteristics showed that occurrence of PMWE were mainly restricted to sunlit time. This fact indicates that electrons detached from negatively charged particles play an important role. While PMWE below 72 km in altitude completely disappeared before sunset, it was detected above that altitude for a few hours even after sunset. This height dependence in the altitude range of 60–80 km can be explained qualitatively by empirical effective recombination rates.

1. Introduction

Polar mesosphere winter echoes (PMWE) are known as mesospheric scattering observed by radars in the polar regions during nonsummer periods and was first identified using a mesosphere-stratosphere-troposphere (MST) radar three decades ago [*Ecklund and Balsley*, 1981]. While a number of MST/ST radars and incoherent scatter (IS) radars have been observing polar mesosphere summer echoes (PMSE), which are closely related to ice particles in the coldest mesopause region [*Cho and Röttger*, 1997; *Rapp and Lübken*, 2004], PMWE are not frequently observed. *Zeller et al.* [2006] conducted the only statistical study reporting on long-term trends of PMWE such as seasonal and interannual variations, which showed that the mean occurrence rate was about 2.9% in a total of 659 day observations. The characteristics in preceding studies can be summarized as follows [*Zeller et al.*, 2006; *Kirkwood*, 2007]: The echo power of PMWE was a few orders of magnitude weaker than that of PMSE. These echoes were typically observed in the altitude range of 60–80 km without a well-defined peak power altitude but often appeared with multiple layers. The PMWE observations were primarily confined to around local noon.

It is well known as a plausible explanation that PMWE are caused by fluctuations in the refractive index due to neutral turbulence associated mainly with breaking of atmospheric gravity waves [*Czechowsky et al.*, 1989; *Brattli et al.*, 2006; *Lübken et al.*, 2007]. This idea is common for most mesosphere echoes and not limited to the polar region [*Czechowsky et al.*, 1979; *Zeller et al.*, 2006]. However, some observations demonstrated that any signatures of turbulence have not been found in most of PMWE layers [*Kirkwood et al.*, 2006a]. For these cases, highly dumped ion acoustic waves induced by reflection of infrasound waves at mesospheric height were suggested [*Kirkwood et al.*, 2006b]. In addition, a simultaneous observation using MST and IS radars showed 1–2 orders of magnitude stronger PMWE than those explained by turbulence alone, which implies the presence of dust particles in PMWE layers[*Belova et al.*, 2005]. Recent radar and artificial electron heating experiments investigated the presence of dust particles and their radius through overshoot effect in PMWE [*Kavanagh et al.*, 2006; *Havnes and Kassa*, 2009].

Another interesting aspect of PMWE is their correlation to significant ionizations in the *D* region triggered by high-energetic particle precipitations such as solar proton event (SPE) and the resultant negative ion chemistry [*Kirkwood et al.*, 2002]. With regard to an electron loss process, electron attachment to dust particles [*Havnes et al.*, 2011; *Friedrich et al.*, 2012] and ion chemical reactions including negative ions [*Kero et al.*, 2008] play a dominant role at PMWE altitudes.

We clarify seasonal variations in PMWE in the Southern Hemisphere (SH) for the first time based on 1 year observations of the Program of the Antarctic Syowa MST/IS (PANSY) radar during austral winter in 2013, because statistical characteristics of PMWE, which are important to understand the dominant generation mechanism of PMWE, still remain poorly known. The PANSY radar has already observed PMWE for 61 and 110 days between June and September 2012 and between March and September 2013, respectively. It should be noted that this study examines whether the height and time characteristics of PMWE in the SH, which were reported only by *Morris et al.* [2011], are common ones to previous studies. We also discuss the occurrence characteristics of PMWE from the viewpoint of solar activity and geomagnetic location of the observation site.

2. Instrumentation

The PANSY radar is a 47 MHz VHF radar installed at Syowa Station, in the Antarctic (69°00′S, 39°35′E) and is being developed toward full system operation. In 2013, mesosphere observations were mostly conducted continuously, except during short periods of system adjustments, with a total antenna aperture of 3900 m^2 (18,000 m^2 for the full system) and peak transmitting power of 113 kW (520 kW for the full system). It was already the largest MST radar in the Antarctic in June 2012 when a quarter system operation started. A more detailed description of the PANSY radar is made by *Sato et al.* [2014]. Observational parameters for the mesosphere are briefly described. Each observation sequence was about 2 min long. Since the observation alternated between the mesosphere mode and the troposphere-stratosphere mode, one data sequence was obtained about every 4 min. The range of measurement was from 60.0 to 97.7 km until the end of May 2013 and was extended to the range from 51.0 to 98.3 km in June 2013, while maintaining a range resolution of 600 m. Five beams in the direction to local zenith, geographic north, east, south, and west with a zenith angle of 10° were formed. The coherent integration time was 12.8 ms, and line-of-sight Doppler velocities were measured to a maximum of $\pm$24.9 m s^{-1}.

3. Results

Figure 1 shows height-time sections of PMWE on 18 May 2013 with time and range resolutions of 4 min and 600 m, respectively. Five panels show the results measured using the five beams. They clearly have almost the same characteristics and variations, suggesting that these echoes were caused not by isolated scatterers but by isotropic scatterers such as Bragg scattering related to atmospheric turbulence. Local noon at Syowa Station on this date was at 0918 UT as indicated by white vertical lines. Around 0630 UT a thin layer with a thickness of $\sim$ 5 km was first observed in the altitude range of 70–75 km. Strong echoes in the altitude range of 60–70 km appeared at 0800 UT and lasted until 1300 UT. After 1300 UT, only weak echoes were detected in the altitude range of 70–75 km, then they completely disappeared around 1600 UT. The sunrise and sunset at 60 km correspond to the solar zenith angle (SZA) of 98° [*Zeller et al.*, 2006], and the SZA at Syowa Station on that day was less than 98° between 0530 and 1310 UT. This means that the onset and disappearance time of PMWE around 70 km were delayed by 1 h and no less than 3 h with respect to the sunrise and sunset, respectively. Note that SPE was identified by the NOAA/GOES spacecraft 3 days before. It is consistent with the report that PMWE were often observed after the sunset during SPE periods [*Zeller et al.*, 2006].

Figure 2a is a probability distribution of echo power measured using all five beams in May 2013. Two populations in Gaussian shape seem to overlap in the distribution. The dominant population with a peak at a low power (−22 dB) seems to correspond to background noise, which was also reported in a previous PMSE study [*Kirkwood et al.*, 2007]. The relatively small population with a peak at a high echo power (−10 dB) is considered to be PMWE. At the first step of analysis, a local minimal value between the two peaks represented by a vertical broken line in the distribution was taken as a lower limit of the PMWE. Echo intensity distributions for respective months from March to September 2013 are plotted in Figure 2b. The shape and

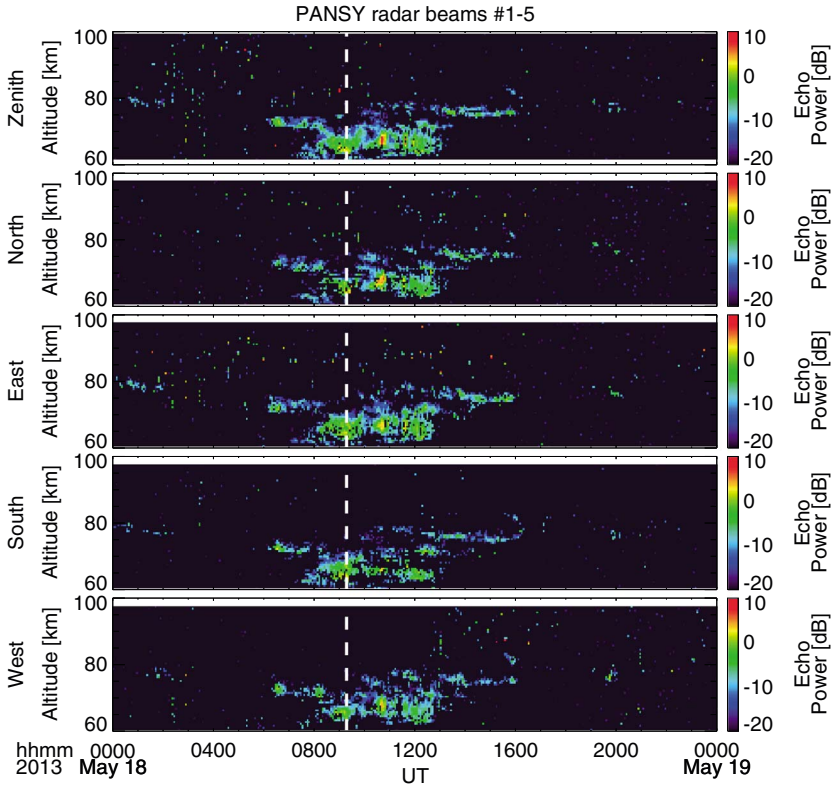

Figure 1. Height-time section of backscattered echo power measured by the PANSY radar in PMWE event on 18 May 2013. Five panels show diurnal variations in PMWE observed with five beams in different directions corresponding to local zenith, geographical north, east, south, and west. White vertical broken lines indicate local noon (0918 UT) on that day.

peak occurrence frequency of the population seems to vary month by month, although the minimum taken as the threshold for PMWE is similarly identified around −15 dB.

To distinguish PMWE from meteor echoes and instantaneous high-power noise, a time fraction occupied by echoes larger than −15 dB in consecutive 15 min observations was used as an additional criterion to identify PMWE [*Czechowsky et al.*, 1989]. If the time fraction was more than a half of the total number of observations in the consecutive 15 min, the region was regarded as one PMWE event. Figures 2c and 2d are the profiles of the number of PMWE and the averaged power for PMWE in May 2013, respectively. The symbols, circle (blue), cross (light blue), triangle (green), diamond (orange), and square (red), correspond to the respective five beams of the PANSY radar. The blue and black curves, respectively, indicate the numbers of PMWE events observed by the vertical beam and the mean numbers for the four off-vertical beams as a function of altitudes. It is seen in Figure 2c that PMWE were observed mainly in the altitude range of 60–77 km with the vertical beam more frequently than by the off-vertical beams by almost 20%. Little PMWE was observed above about 80 km by any beams. In contrast, the monthly mean echo power profiles of PMWE in Figure 2d do not have a significant difference less than 2 dB among the beams below 80 km. Note that when the number of samples was smaller than 60, the mean power was not plotted in order to exclude the effect of meteor echoes above 80 km.

Figure 2e shows a daily occurrence rate of PMWE as a function of time from 1 March to 31 October 2013. The red and black curves show the occurrence rate calculated for the altitude range of 60–80 km and its 27 day running average, respectively. There are many enhancements superimposed on the seasonal variations that are maximized in the middle of May. During the observation period, SPE occurred 6 times, as indicated by black arrows. Two abrupt increases in the occurrence rate reaching 10% in the last half of May may be related to the two SPEs. However, it seems that the SPE at the end of September that was the second largest during the period and does not seem to affect the occurrence rates. This implies that PMWE are not

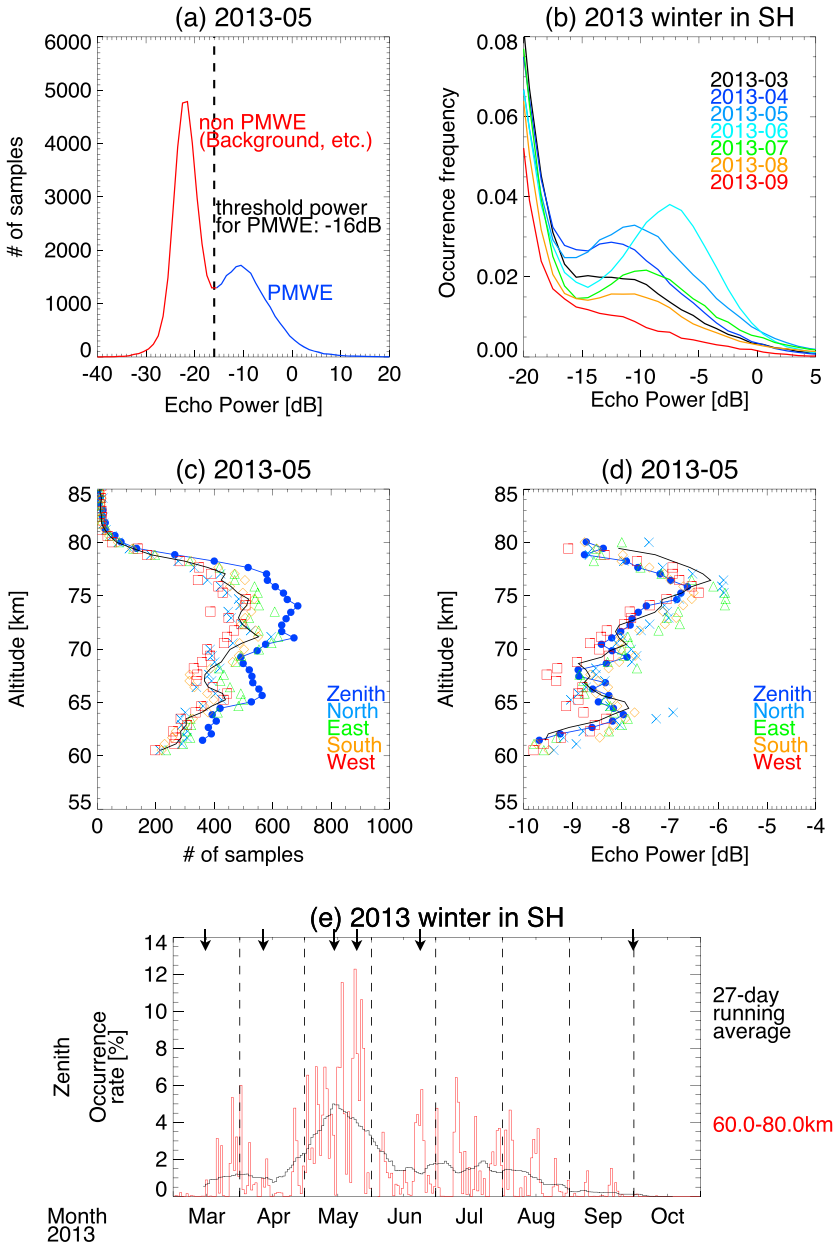

Figure 2. (a) Histogram of echo power at all ranges between 60.0 and 97.7 km measured by the PANSY radar in May 2013. Vertical broken line represents echo power threshold for PMWE in that month. (b) Similar plot in occurrence frequency for each month between March and September 2013. Horizontal axis is limited to range from −20 to +5 dB. Colors indicate different months. (c) Monthly mean height profile of number of PMWE events. Five symbols in different colors indicate respective beams of the PANSY radar. Black curve shows averaged profile of four off-vertical beams. (d) Monthly mean profile in same format but for echo power associated with only PMWE. Data above altitude of 80 km were not plotted (see text). (e) Daily occurrence rate of PMWE as a function of time from March to October 2013 (red curve) and 27 day running average of daily occurrence (black curve). Black arrows at top of figure indicate onsets of SPE.

necessarily accompanied by SPE; thus, turbulence controls the intensity of PMWE as well as electron density, as pointed out by *Lübken et al.* [2006].

We further investigated the statistical characteristics of PMWE. Figure 3a shows the monthly mean of echo power including all echoes as functions of UT and altitude. We calculated averaged echo power for boxes with a height width of 600 m and a time width of 10 min. It is seen that in Figure 3a that much noise and contamination from meteor echoes still remained at all local times above 75 km. Figure 3b is the same as Figure 3a but for the results using the data identified as PMWE only. The occurrence rate of the echoes

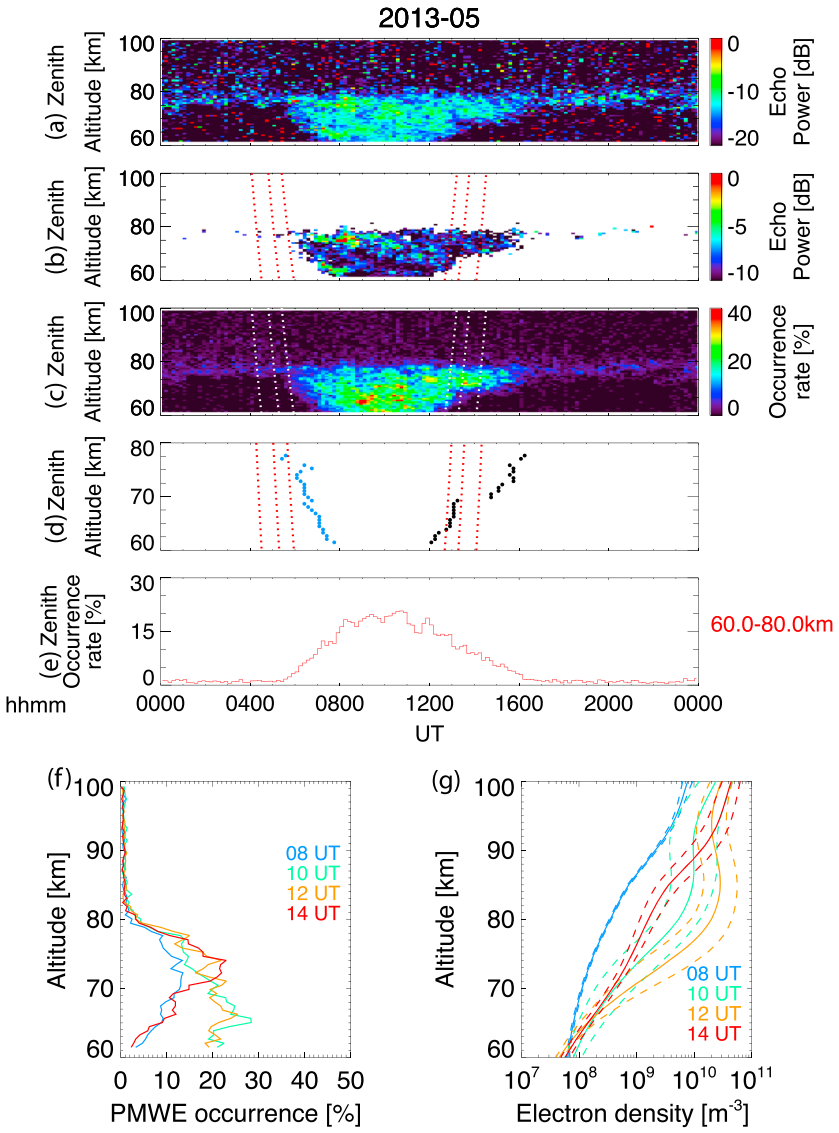

Figure 3. Monthly mean of diurnal variations for (a) all echo power, (b) PMWE power, and (c) occurrence rates of PMWE, in May 2013. Minimum box was with a height width of 600 m and a time width of 10 min. (d) Height dependence of PMWE appearance and disappearance time indicated by light blue and black dots, respectively. Appearance and disappearance time are picked up as time when the occurrence rates at each altitude are closest to 20% of the maximum rate. Dotted lines in Figures 3b–3d represent sunrise and sunset times, respectively, for each altitude on 1, 16, and 31 May. (e) Diurnal variations of occurrence rates over range from 60.0 to 80.0 km altitude. (f) Monthly mean of PMWE occurrence rates as a function of altitudes. Colors indicate different UT (0800, 1000, 1200, and 1400 UT). (g) Monthly mean of electron density profiles (solid) with standard deviations (broken) based on IMAZ [*McKinnell and Friedrich*, 2007].

is plotted in Figure 3c. Note that the data in which the number of samples is less than 7 (corresponds to occurrence rate of $\leq$ 6% in Figure 3c) were not plotted in Figure 3b in order to remove contamination of meteor echoes. Figures 3b and 3c clearly show interesting statistical characteristics of PMWE in the height and UT sections. A clear upper boundary was located around 80 km independent of UT, which agrees with the altitude above which turbulence with a scale of 3 m is significantly damped [*Hocking*, 2011]. Two enhanced echo regions are observed in the altitude range of 62–63 km and of 74–76 km just after PMWE onset as seen in Figure 3b.

In addition, the PMWE occurrence rate is asymmetric against local noon (~ 0920 UT). Figure 3d shows PMWE appearance time and disappearance one indicated by light blue and black dots as a function of height, respectively. The inclined dotted lines in Figures 3b–3d represent the time of sunrise and sunset at each

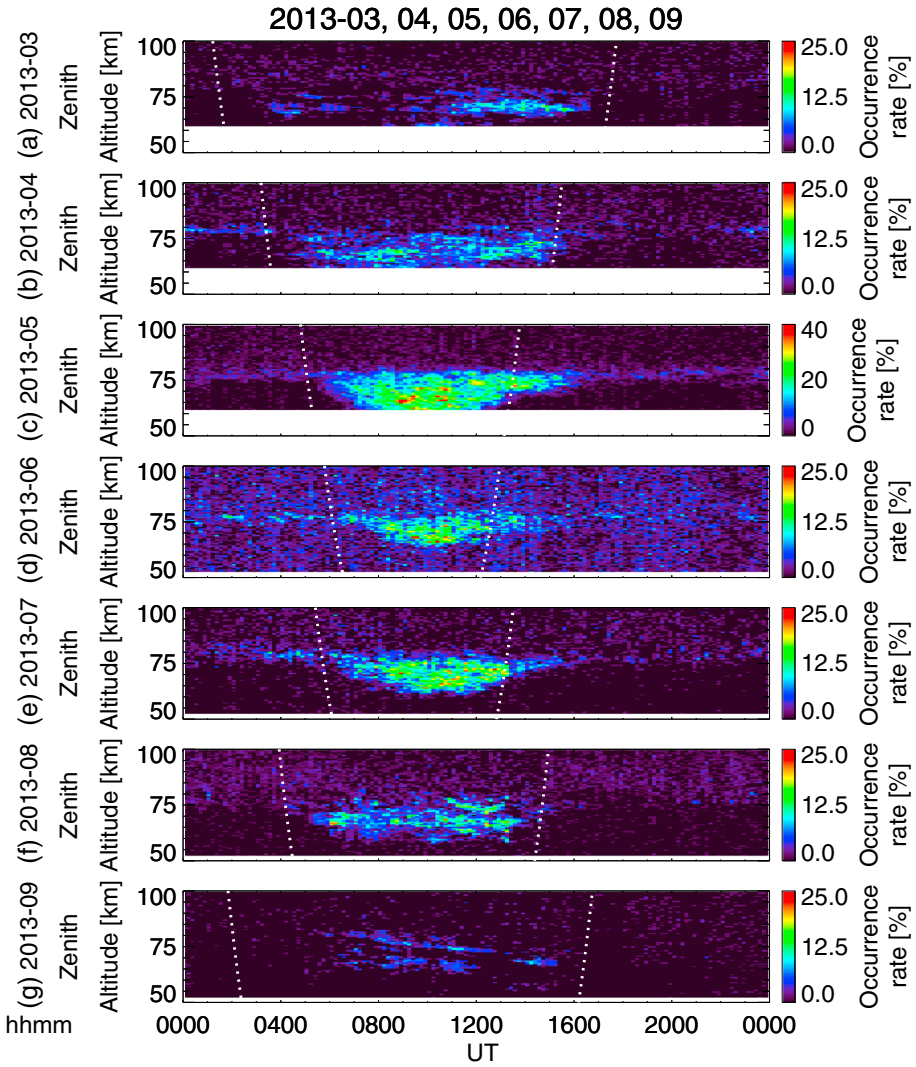

Figure 4. Summary plot for seasonal variations in monthly mean of PMWE characteristics from March to September 2013. Note that color scale for rates used in May is different from those in other months. White dotted lines indicate sunrise and sunset times in middle day of each month.

altitude on 1, 16, and 31 May. As shown in Figure 3d, it is clear that the onset of PMWE in the altitude range of 60–75 km was delayed by 1–3 h with respect to sunrise. Additionally, the delay time of onset was larger for the lower altitude. On the other hand, PMWE below 72 km disappeared earlier than sunset, although PMWE in the altitude range of 72–77 km extended to the nightside and remained even after sunset. The delay time became longer at higher altitudes and reached 2–3 h near 77 km. Figure 3e shows diurnal variations in occurrence rate in the altitude range of 60–80 km in May. It indicates that PMWE started to appear at 0600 UT and stayed in the peak around local noon (0800–1200 UT), as reported by *Zeller et al.* [2006]. From 1200 to 1600 UT, PMWE disappeared more gradually than when they appeared.

We compared time and height variations in the disappearance of PMWE with electron density calculated by Ionospheric Model for the Auroral Zone (IMAZ) [*McKinnell and Friedrich*, 2007]. Figures 3f and 3g show the profiles of monthly mean of PMWE occurrence rates and IMAZ electron density at different UT in May 2013. Note that IMAZ is required for input of *Ap* index. But optional input parameter of riometer absorption was not used in this calculation. The modeled electron density at 1400 UT shows relatively large values of 10^8–10^9 m^{-3} above 70 km, which implies that high electron density before sunset (≈ 1400 UT) was produced by the two SPEs in this month. This is consistent with that occurrence rate of PMWE above 72 km

did not change much from 1200 to 1400 UT. On the other hand, the electron density of IMAZ cannot explain PMWE occurrence rate below 70 km from 0800 to 1400 UT.

Finally, height-time sections of the monthly mean PMWE in March through September 2013 are presented in Figure 4 in order to examine seasonal variability. The seasonal behavior of PMWE can be identified, although the plot for June is somewhat noisy. PMSE almost disappeared in March, whereas PMWE started to be observed below 80 km. A very high occurrence rate of 20–30% was obtained in May, and this may be related to the two SPEs in the last half of May. The PMWE totally disappeared in September, and neither PMWE nor PMSE were observed at all in October (not shown). The white dotted lines represent the moment of sunrise and sunset at each altitude in the middle of each month. It is clear that the mean duration of PMWE strongly depended on the sunlit time. The delay in onset time with respect to sunrise was commonly seen in all months, except for the thin echo layer which was identified around 75 km in June and July. On the other hand, extended PMWE after sunset are clearly identified above 70 km for May, June, and July in spite of their short sunlit time. The upper and lower boundaries of PMWE seen near 80 and 60 km, respectively, seem to be stable in all months.

4. Discussion and Conclusions

We reported day-to-day variations in PMWE occurrence rates as a function of day in 2013, as shown in Figure 2e. While the highest rate was 11% for SPE on 24 May, *Morris et al.* [2011] reported that it was 10 % during SPE in 2005. On the other hand, PMWE above Syowa Station were more frequently detected by the PANSY radar from March to September, even during periods without any SPE. This is because antenna effective area and peak power of the PANSY radar from March to September 2013 were 1.8 and 3.1 times as large as those of the MST radar in Davis Station, respectively. In addition to the difference in the performances of the two radars, the difference in geomagnetic location between the two stations is also important. The magnetic latitude (MLAT) of Syowa Station is 70.4°; therefore, it is usually located under the auroral oval connecting to the source of precipitating electrons in the energy range from 1 keV to 30 keV [*Newell et al.*, 2009], and even to approximately a few hundred keV. In contrast, energetic particle precipitations except for SPE are not expected to occur frequently at Davis Station where the MLAT is 74.4°. Although neutral turbulence is required for PMWE to be detected, volume reflectivity is more sensitive to electron density than the turbulent energy dissipation rate [*Lübken et al.*, 2006; *Kero et al.*, 2008]. In addition, electron density in the mesosphere can vary from less than 10^8 up to 10^{10} m^{-3} day to day [*Kirkwood et al.*, 2002]. Contributions from electron density variation by solar radiation and particle precipitations as well as turbulence intensity variation should be quantitatively evaluated through comprehensive observations.

Although *Ecklund and Balsley* [1981] already reported that PMWE at higher altitudes disappeared after sunset, the height dependence of PMWE appearance/disappearance was not fully discussed likely because of the insufficient height resolution of 2.2 km in their study. As shown in Figure 3d, the present study with the 600 m height resolution revealed that PMWE below 72 km completely disappeared before sunset and PMWE above that altitude was still detected after sunset in May, June, and July 2013. A plausible candidate for the quick disappearance at the altitude range of 60–72 km is meteor smoke particles (MSP) with a radii of a few nanometers [*Havnes and Kassa*, 2009]. It was suggested that MSP acts as a strong sink for electrons during the night [*Havnes et al.*, 2011]. On the other hand, above 72 km PMWE was detected after sunset as shown in Figures 3d, which implies that electron loss rates are different between below and above 72 km. In situ measurements by rockets in *Thrane et al.* [1979] demonstrated that the electron loss rate gradually decreased with height from 10^{-10} m^3 s^{-1} near 65 km to 10^{-11} m^3 s^{-1} near 75 km, and rapidly decreased to 10^{-12} m^3 s^{-1} around 78 km; therefore, the timescale of electron loss becomes longer for the altitude higher than 75 km. This height dependence of effective electron loss rates qualitatively agrees with the observed time and height characteristic of PMWE disappearance.

To examine how long PMWE can exist around 77 km after sunset, we conducted an order estimation of time scale for electron loss. The continuity equation of electrons ignoring transport effects can be written as follows:

$$\frac{dn_e}{dt} = Q - \alpha_{\mathrm{eff}} \cdot n_e^2$$

where n_e is electron density, Q is electron production rates per unit volume by photoionization and detachment from negatively charged particles, and α_{eff} is effective electron recombination rates [*Thrane et al.*, 1979;

Friedrich et al., 2004]. Considering after-sunset time, i.e., $Q \approx 0$, electron density as a function of time can be estimated as follows:

$$n_e = \frac{n_{e0}}{1 + t/\tau_e}, \quad \text{where} \quad \tau_e = \frac{1}{n_{e0} \cdot \alpha_{\text{eff}}}$$

For the case that initial electron density, n_{e0}, is sufficiently larger than n_e, the equation can be simplified as

$$t = \frac{n_{e0} - n_e}{n_e} \cdot \frac{1}{\tau_e} = \frac{n_{e0} - n_e}{n_{e0}} \cdot \frac{1}{n_e \cdot \alpha_{\text{eff}}} \approx \frac{1}{n_e \cdot \alpha_{\text{eff}}}$$

Here we assume that the electron density at sunset, n_{e0}, is $\geq 10^8$ m^{-3} that is consistent with that of IMAZ model. Empirical α_{eff} near 80 km after sunset was determined as $\sim 10^{-11}$ m^3 s^{-1} [*Friedrich et al.*, 2004]. By using this α_{eff} and n_e of 10^7 m^{-3}, which is a normal electron density in nighttime calculated by IMAZ model, the required time is roughly 10^4 s. This timescale is consistent with the observation in which PMWE remained for a few hours after sunset. Actual electron density and effective recombination rates around 80 km during PMWE occurrence should be evaluated by comparisons with in situ measurements or chemical models taking into account ionizations due to energetic particle precipitations. Although atmospheric composition and its height variability in the mesosphere are important to understand the nature of PMWE, it is beyond the scope of this study and should be addressed in the future.

We presented the monthly mean characteristics of PMWE and their seasonal variability based on 1 year data set by using the PANSY radar and a statistical analysis method. PMWE occurrence frequency during austral winter in 2013 was at its peak in the middle of May when two SPE occurred. PMWE were also observed even during periods without any SPE, suggesting a possible cause of the PMWE is ionization by energetic electrons precipitations. The delay of PMWE onset with respect to sunrise ranging from 1 to 2 h was observed in May, June, and July 2013, which is consistent with the idea that free electrons are mainly produced by the detachment from negative ions under an SZA $< 98°$ [*Friedrich et al.*, 2004; *Zeller et al.*, 2006] and negative MSPs [*Rapp*, 2009; *Havnes et al.*, 2011]. We also revealed that PMWE has height dependence in the altitude range of 60–80 km and its transition height near 72 km, which can be explained qualitatively by the height dependence of electron loss rate.

Acknowledgments

This study is supported by Grant-in-Aid for Scientific Research (A) 25247075 and (B) 24340121 of the Ministry of Education, Culture, Sports, Science, and Technology (MEXT), Japan, and KP-2 project of National Institute of Polar Research. The PANSY radar was operated by Japanese Antarctic Research Expedition (JARE), and the authors greatly appreciate the continuous support from all JARE members. PANSY is a multi-institutional project with a core of the University of Tokyo and National Institute of Polar Research. The PANSY radar observation data are available at the project website, http://pansy.eps.s.u-tokyo.ac.jp. The information of SPE is available in the following address: ftp://ftp.swpc.noaa.gov/pub/indices/SPE.txt. The production of this paper was supported by an NIPR publication subsidy.

The Editor thanks David Rusch and an anonymous reviewer for their assistance in evaluating this paper.

References

Belova, E., S. Kirkwood, J. Ekeberg, A. Osepian, I. Häggström, H. Nilsson, and M. Rietveld (2005), The dynamical background of polar mesosphere winter echoes from simultaneous EISCAT and ESRAD observations, *Ann. Geophys.*, *23*, 1239–1247.

Brattli, A., T. A. Blix, Ö. Lie-Svendsen, U.-P. Hoppe, F. J. Lübken, M. Rapp, W. Singer, and M. Friedrich (2006), Rocket measurements of positive ions during polar mesospheric winter echoes, *Atmos. Chem. Phys.*, *6*, 5515–5524.

Cho, J. Y. N., and J. Röttger (1997), An updated review of polar mesosphere summer echoes: Observation, theory, and their relationship to noctilucent clouds and subvisible aerosols, *J. Geophys. Res.*, *102*, 2001–2020.

Czechowsky, P., R. Rüster, and G. Schmidt (1979), Variations of mesospheric structures in different seasons, *Geophys. Res. Lett.*, *6*, 459–462, doi:10.1029/GL006i006p00459.

Czechowsky, P., I. M. Reid, R. Rüster, and G. Schmidt (1989), VHF radar echoes observed in the summer and winter polar mesosphere over Andöya, Norway, *J. Geophys. Res.*, *94*(D4), 5199–5217, doi:10.1029/JD094iD04p05199.

Ecklund, W. L., and B. B. Balsley (1981), Long-term observations of the Arctic mesosphere with the MST radar at Poker Flat, Alaska, *J. Geophys. Res.*, *6*, 7775–7780, doi:10.1029/JA086iA09p07775.

Friedrich, M., K. M. Torkar, and R. J. Steiner (2004), Empirical recombination rates in the lower ionosphere, *Adv. Space Res.*, *34*, 1937–1942.

Friedrich, M., M. Rapp, T. Blix, U.-P. Hoppe, K. Torkar, S. Robertson, S. Dickson, and K. Lynch (2012), Electron loss and meteoric dust in the mesosphere, *Ann. Geophys.*, *30*, 1495–1501, doi:10.5194/angeo-30-1495-2012.

Havnes, O., and M. Kassa (2009), On the sizes and observable effects of dust particles in polar mesospheric winter echoes, *J. Geophys. Res.*, *114*, D09209, doi:10.1029/2008JD011276.

Havnes, O., C. La Hoz, M. T. Rietveld, M. Kassa, G. Baroni, and A. Biebricher (2011), Dust charging and density conditions deduced from observations of PMWE modulated by artificial electron heating, *J. Geophys. Res.*, *116*, D24203, doi:10.1029/2011JD016411.

Hocking, W. K. (2011), A review of mesosphere-stratosphere-troposphere (MST) radar developments and studies, circa 1997–2008, *J. Atmos. Sol. Terr. Phys.*, *73*, 848–882, doi:10.1016/j.jastp.2010.12.009.

Kavanagh, A. J., F. Honary, M. T. Rietveld, and A. Senior (2006), First observations of the artificial modulation of polar mesosphere winter echoes, *Geophys. Res. Lett.*, *33*, L19801, doi:10.1029/2006GL027565.

Kero, A., J. Vierinen, C.-F. Enell, I. Virtanen, and E. Turunen (2008), New incoherent scatter diagnostic methods for the heated D-region ionosphere, *Ann. Geophys.*, *26*, 2273–2279.

Kirkwood, S. (2007), Polar mesosphere winter echoes: A review of recent results, *Adv. Space Res.*, *40*, 751–757, doi:10.1016/j.asr.2007.01.024.

Kirkwood, S., V. Barabash, E. Belova, H. Nilsson, T. N. Rao, K. Stebel, A. Osepian, and P. B. Chilson (2002), Polar mesosphere winter echoes during solar proton events, *Adv. Polar Upper Atmos. Res.*, *16*, 111–125.

Kirkwood, S., E. Belova, U. Blum, C. Croskey, P. Dalin, K. H. Fricke, R. A. Goldberg, J. Manninen, J. D. Mitchell, and F. Schmidlin (2006a), Polar mesosphere winter echoes during MaCWAVE, *Ann. Geophys.*, *24*, 1245–1255, doi:10.5194/angeo-24-1245-2006.

Kirkwood, S., P. Chilson, E. Belova, P. Dalin, I. Häggström, M. Rietveld, and W. Singer (2006b), Infrasound: The cause of polar mesosphere winter echoes?, *Ann. Geophys.*, *24*, 475–491, doi:10.5194/angeo-24-475-2006.

Kirkwood, S., I. Wolf, H. Nilsson, P. Dalin, D. Mikhaylova, and E. Belova (2007), Polar mesosphere summer echoes at Wasa, Antarctica (73°S): First observations and comparison with 68°N, *Geophys. Res. Lett.*, *34*, L15803, doi:10.1029/2007GL030516.

Lübken, F.-J., B. Strelnikov, M. Rapp, W. Singer, R. Latteck, A. Brattli, U. P. Hoppe, and M. Friedrich (2006), The thermal and dynamical state of the atmosphere during polar mesosphere winter echoes, *Atmos. Chem. Phys.*, *6*, 13–24, doi:10.5194/acp-6-13-2006.

Lübken, F.-J., W. Singer, R. Latteck, and I. Strelnikova (2007), Radar measurements of turbulence, electron densities, and absolute reflectivities during Polar Mesosphere Winter Echoes (PMWE), *Adv. Space Res.*, *40*, 758–764.

McKinnell, L.-A., and M. Friedrich (2007), A neural network-based ionospheric model for the auroral zone, *J. Atmos. Sol. Terr. Phys.*, *69*, 1459–1470, doi:10.1016/j.jastp.2007.05.003.

Morris, R. J., A. R. Klekociuk, and D. A. Holdsworth (2011), First observations of Southern Hemisphere polar mesosphere winter echoes including conjugate occurrences at ∼69°S latitude, *Geophys. Res. Lett.*, *38*, L03811, doi:10.1029/2010GL046298.

Newell, P. T., T. Sotirelis, and S. Wing (2009), Diffuse, monoenergetic, and broadband aurora: The global precipitation budget, *J. Geophys. Res.*, *114*, A09207, doi:10.1029/2009JA014326.

Rapp, M. (2009), Charging of mesospheric aerosol particles: The role of photodetachment and photoionization from meteoric smoke and ice particles, *Ann. Geophys.*, *27*, 2417–2422.

Rapp, M., and F.-J. Lübken (2004), Polar mesosphere summer echoes (PMSE): Review of observations and current understanding, *Atmos. Chem. Phys.*, *4*, 2601–2633.

Sato, K., M. Tsutsumi, T. Sato, T. Nakamura, A. Saito, Y. Tomikawa, K. Nishimura, M. Kohma, H. Yamagishi, and T. Yamanouchi (2014), Program of the Antarctic Syowa MST/IS radar (PANSY), *J. Atmos. Sol. Terr. Phys.*, *118*, 2–15, doi:10.1016/j.jastp.2013.08.022.

Thrane, E. V., B. Grandal, O. Hagen, F. Ugletveit, W. Bangert, M. Friedrich, A. Loidl, H. Schwentek, and K. M. Torkar (1979), Ion production and effective loss rate in the mesosphere and lower thermosphere during the western European winter anomaly campaign 1975/76, *J. Atmos. Terr. Phys.*, *41*, 1097–1103.

Zeller, O., M. Zecha, J. Bremer, R. Latteck, and W. Singer (2006), Mean characteristics of mesosphere winter echoes at mid- and high-latitudes, *J. Atmos. Sol. Terr. Phys.*, *68*, 1087–1104, doi:10.1016/j.jastp.2006.02.015.